# Observational Verification of Hierarchical Evolution Models in Galactic Molecular Clouds

Kotora Sasaki, Nario Kuno, Hajime Fukushima, Shinji Fujita, Shingo Nozaki

# 1. Introduction

## Cloud-Cloud Collision (CCC)

Massive Stars ( $> 8\ M_\odot$ )

Key drivers of galactic evolution (via UV radiation, feedback)

**Formation mechanism remains an open question.**

Cloud-Cloud Collision (CCC) Scenario

A promising trigger for massive star formation.

Supported by numerous observations (e.g., Fujita et al. 2021)

The Timescale Discrepancy (Sun et al. 2022)

- Collision timescale : ~ 100 Myr
- Cloud free-fall time : 5 - 20 Myr

→ **Random collisions should be events.**

**Revealing the mechanism driving frequent CCC is essential to understanding massive star formation.**

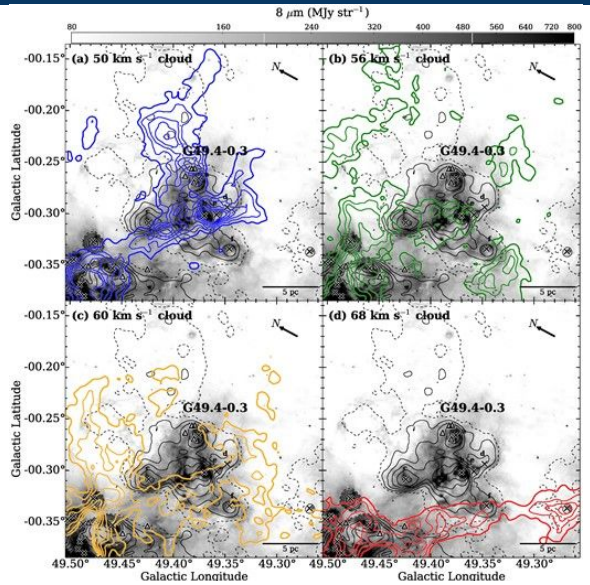


Fujita et al. 2021

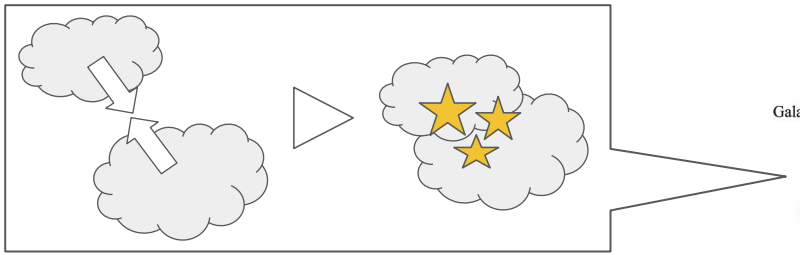

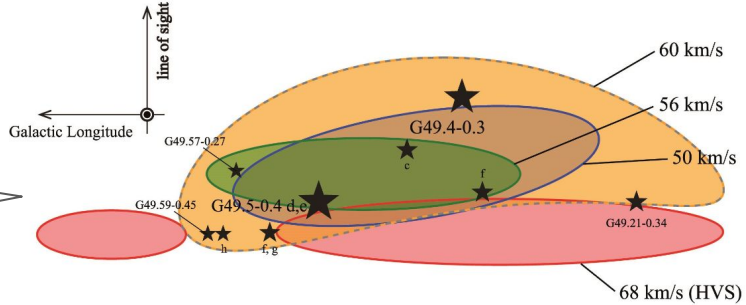

# 1. Introduction

## Global Hierarchical Collapse (GHC)

Global Hierarchical Collapse
(GHC, e.g., V´azquez-Semadeni et al. 2019)

Global contraction of GMCs
→ Herarchical formation of dense structures inside

**Collisions and interactions of dense structures efficiently trigger massive star formation.**

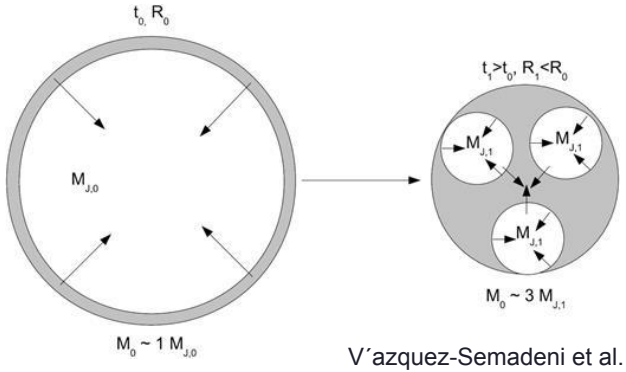


V´azquez-Semadeni et al. 2019

Previous Studies

- Maddalena GMC (Shen et al. 2024)
  Comparision of physical properties between hierarchical and monolithic structures
- Rosette molecular cloud (He et al. 2026)
  Global structure supports the GHC model.

Previous studies are limited to single case studies.
**Is GHC universal across many molecular clouds in the Galaxy?**

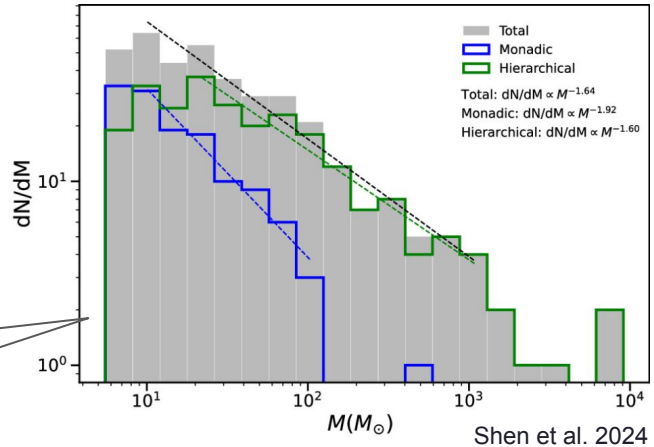


Shen et al. 2024

Difference in mass distribution between hierarchical (green) and monolithic (blue) structures in Maddalena GMC

# 1. Introduction

## Aims

**Main goal: Systematically evaluate the relationship between hierarchical structures and star formation activity across multiple molecular clouds in the Galaxy**

- Data: FUGIN project (Nobeyama 45m telescope; Umemoto et al. 2017)
- Algorithm: Apply Dendrogram (Rosolowsky et al. 2008) to extract hierarchical structures
- Discuss formation and evolutionary processes based on physical properties derived from these structures

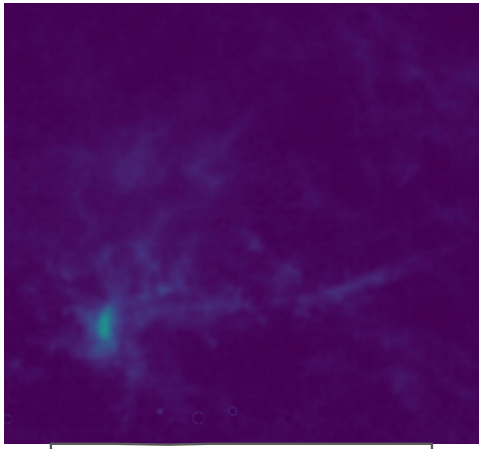

FUGIN Data

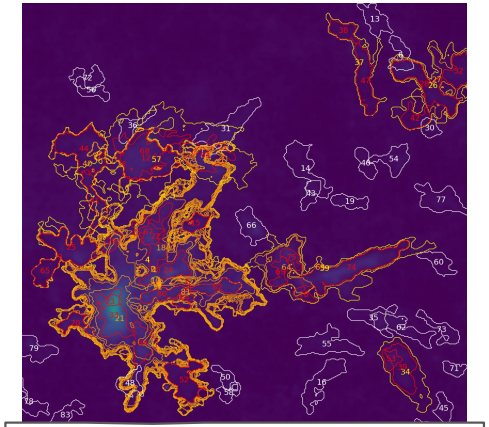

Structure Extraction via Dendrogram

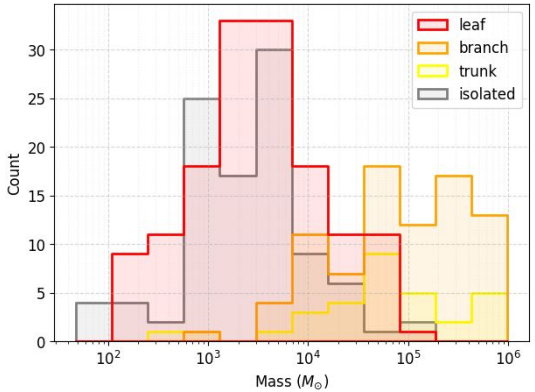


Calculation of Physical Properties & Discussion

# 2. Data

## FUGIN

FUGIN Project

（FOREST Unbiased Galactic plane Imaging survey with the Nobeyama 45m telescope, Umemoto et al. 2017）

Large-scale simultaneous survey of CO isotopologues in the Galactic plane

High Angular Resolution：~ 20", Velocity Resolution：1.3 km $s^{-1}$

Target Line: $^{13}$CO($J$ = 1-0)（**Optically thin tracer suitable for probing internal cloud structures**）

Target Regions: Selected 12 candidate regions for CCC / GHC analysis

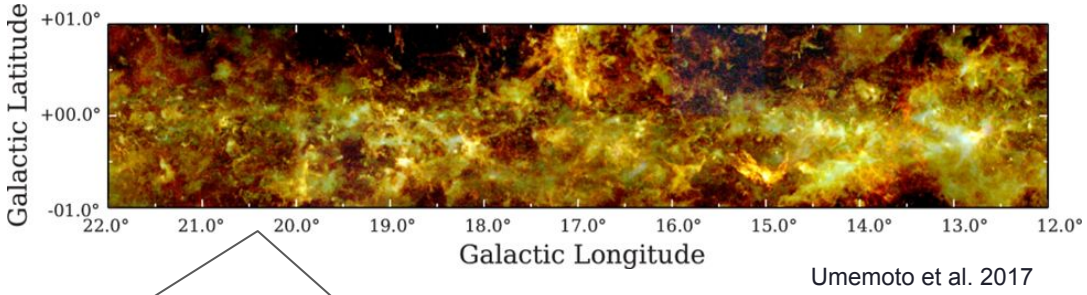


Umemoto et al. 2017

Three-color composite image of $^{12}$CO, $^{13}$CO, C$^{18}$O($J$ = 1-0)

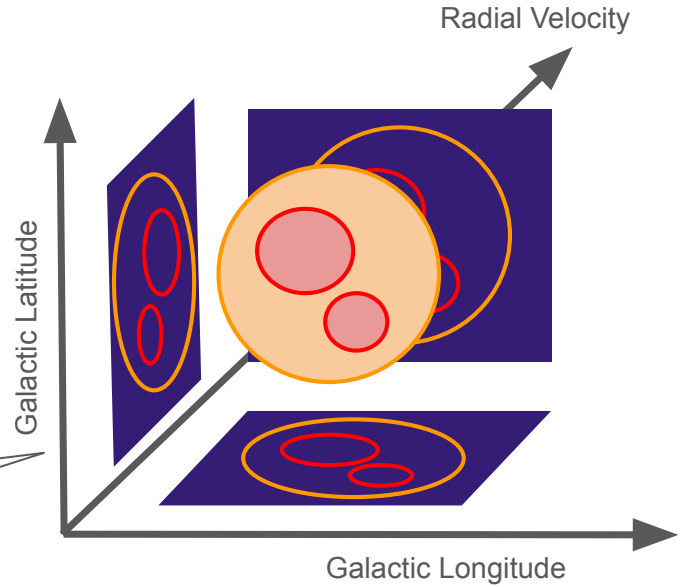


Extraction of 3D hierarchical structures from the (*l, b, v*) data cube
Visualization via projection onto 2D planes

# 3. Analysis Tool

## Dendrogram

Dendrogram algorithm（Rosolowsky et al. 2008）
Identifies hierarchical structures in 3D data cubes based on emission intensity

- Leaf: Smallest unit with no substurcture
- Branch: Structure containing substurctures
- Trunk: Top-level structure (largest scale)
- Isolated: Single structure with no parent or child (used for comparison)

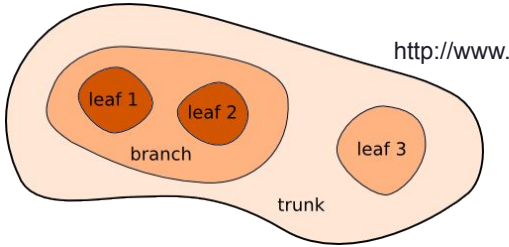


http://www.dendrograms.org/

Derivation of Physical Properties

- Effective Radius ( $R$ ): Derived from projected area ( $S$ ) $R = \sqrt{S/\pi}$
- Mass ( $M$ ): Derived from $H_2$ column density ( $N_{H_2}$ ) assuming LTE ( $M = \mu m_{\mathrm{H}} A_{\mathrm{pix}} \sum N_{\mathrm{H}_2}$ )
- Volume Density ( $\rho$ ): Assumed spherical symmetry ( $\rho = \frac{M}{V} \quad V = \frac{4}{3}\pi R^3$ )
- Virial Parameter ( $\alpha_{\mathrm{vir}}$ ): Derived from velocity dispersion ( $\sigma_v$ ) $\alpha_{\mathrm{vir}} = \frac{5\sigma_v^2 R}{GM}$

$\mu = 2.8$ Mean molecular weight
$m_{\mathrm{H}}$ Mass of hyudorgen atom
$A_{\mathrm{pix}}$ Physical area of one pixel

Evaluate the balance between gravity and turbulence (Bertoldi & McKee 1992)

# 4. Results

## Histogram of Physical Quantities of The Entire Structure

Leaf (Hierarchical) vs. Isolated (Monolithic)

Effective Radius: No significant difference
Mass, Volume Density : **Leaf > Isolated**
Virial Parameter : **Leaf < Isolated**

→ **Hierarchical structures (Leaves) provide a more favorable environment for star formation compared to isolated structures.**

| Physical Quantity | p-value |
|---|---|
| Effective Radius | 0.52 |
| Mass | $2.1 \times 10^{-6}$ |
| Volume Density | $2.6 \times 10^{-9}$ |
| Virial Parameter | $4.1 \times 10^{-4}$ |

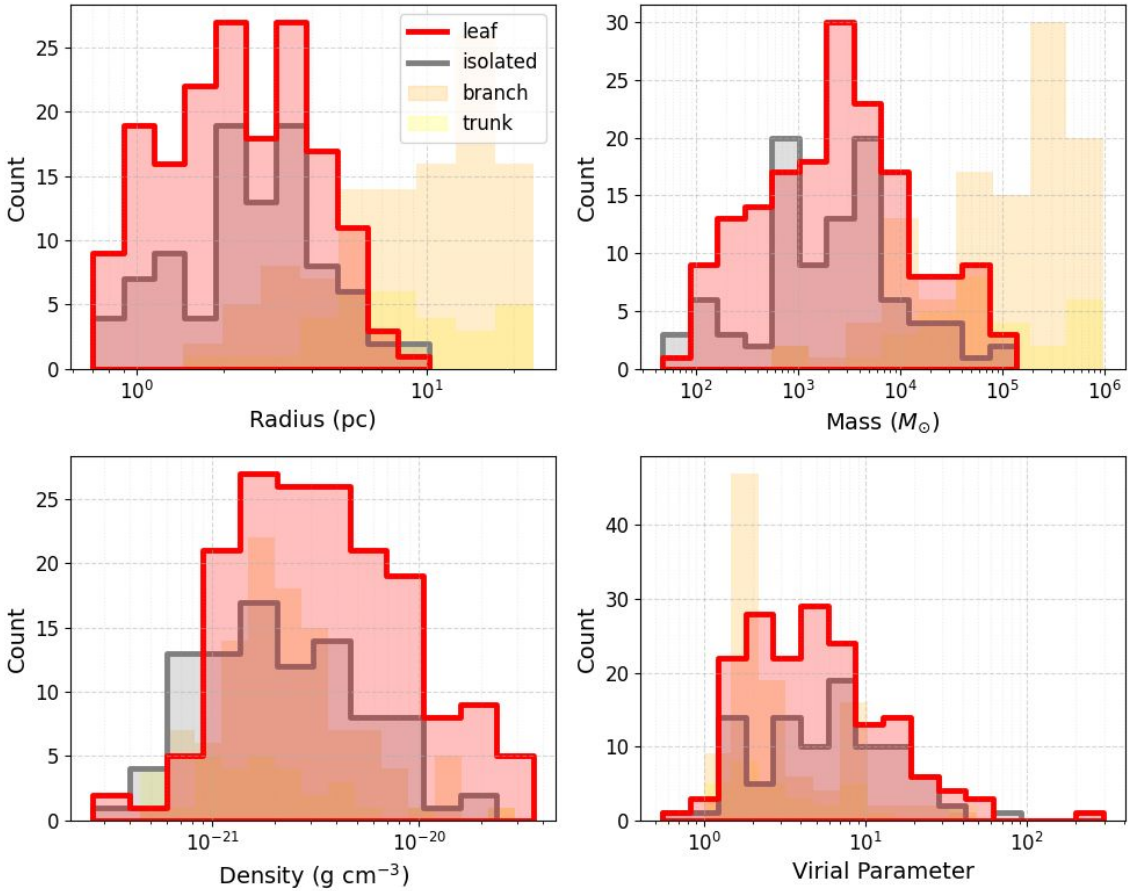

# 4. Results

## Analysis Results of W51A

Physical Properties in W51A

- Hierarchical structures are denser and have significantly lower virial parameter compared to isolated structures (p = 0.012).

→ **Hierarchical structures provide a favorable environment for star formation, consistent with global statistics.**

Kinematics Structure (Position-Velocity Diagram)

- Leaves: Distributed across multiple velocity components
- Branches / Trunks: Span across these different velocity components

→ **Evidence of hierarchical confinement structures that induce collisions between dense structure (CCC).**

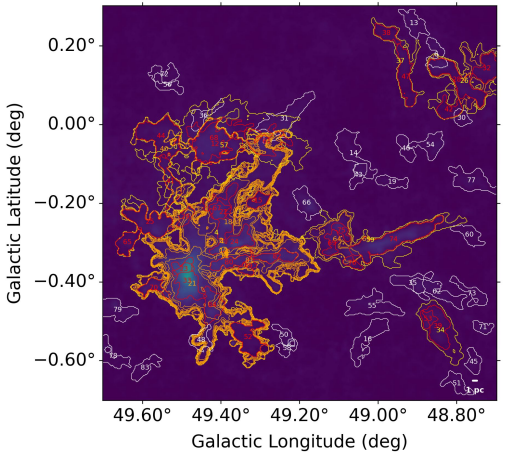


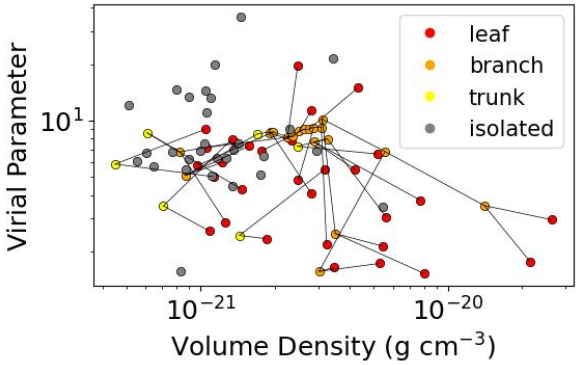


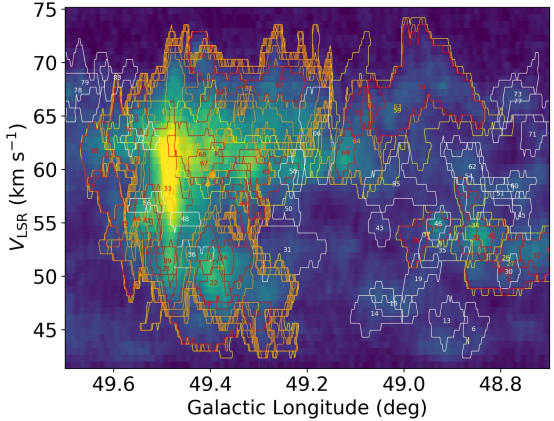


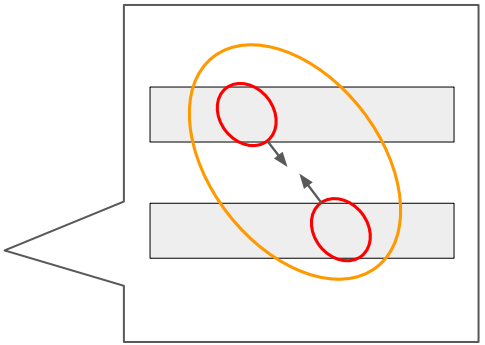

# 5. Discussion

## Comparison with MIR Data

Overlay of dendrogram contours on Spitzer 8 μm / 24 μm images

→ **Hierarchical structures spatially coincide with active star-forming regions.**

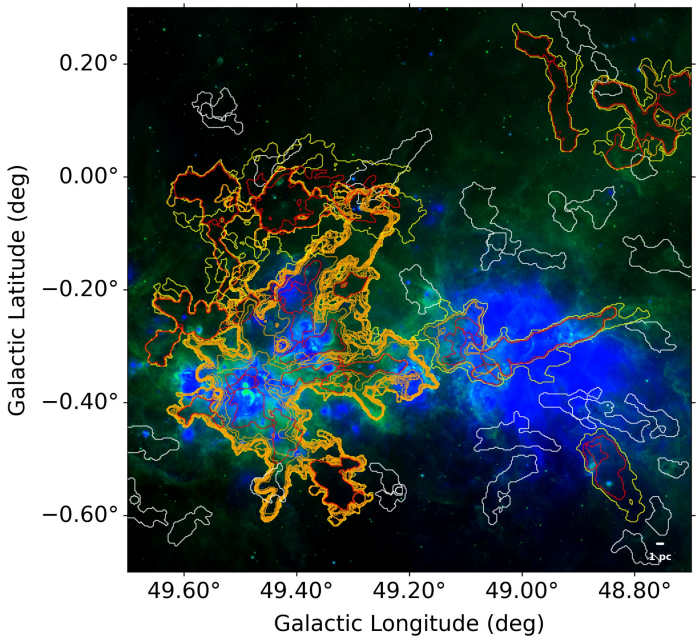


Density vs. IR Intensity

Volume density is proportional to IR intensity.

Hierarchical structures exhibit higher IR emission than isolated ones (Hierarchical ≧ isolated)

→ **Active star formation is ongoing within the high-density hierarchical structures.**

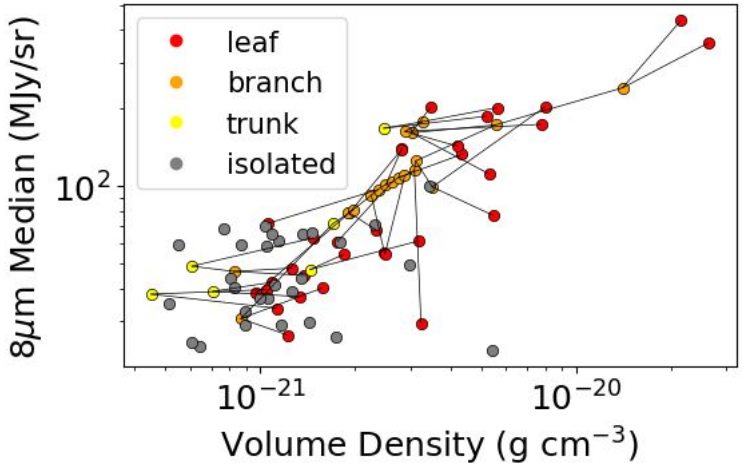

# 5. Discussion

## Comparison with HII Catalog

Number of Associated HII Regions

Leaf (Max 10) > Isolated (Max 3)

→ **Hierarchical structures (Leaf) host significantly more HII regions.**

Fraction of HII Region Association

No significant difference depending on physical properties

→ **The physical conditions required to trigger massive star formation are similar.**

・Isolated (High Virial)

Vulnerable to feedback

→ Gas dispersal → **Formation halts.**

・Hierarchical (Low Virial)

Confinement by external layers

→ Gas retention → **Formation sustained.**

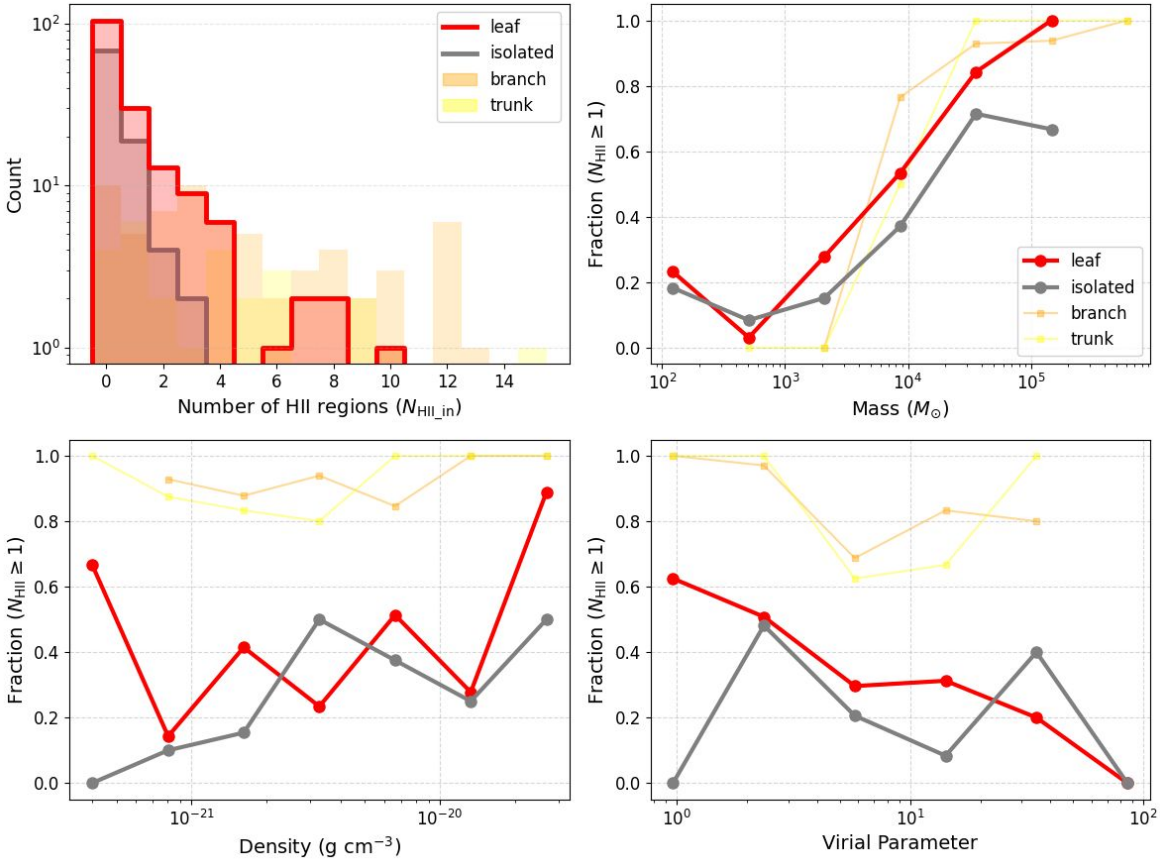

# 5. Discussion

## Possible Hierarchical Evolutionary Scenarios

1. **Global Contraction (Trunk)**
   Contraction of the entire cloud (Trunk)
   Generates diverse velocity components internally

2. **Hierarchical Formation (Leaf)**
   Formation of leaves with distinct porper motions during global contraction

3. **Confinement & Interaction**
   Trunk maintains high density environment.
   Collisions between leaves trigger massive star formation.

4. **Resistance to Feedback**
   Confinement suppresses gas dispersal.
   → Sustains Clustered Star Formation

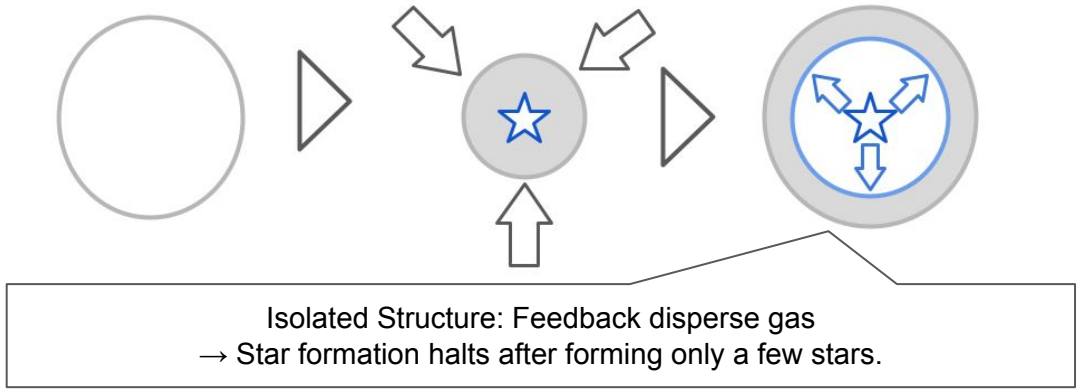

Isolated Structure: Feedback disperse gas
→ Star formation halts after forming only a few stars.

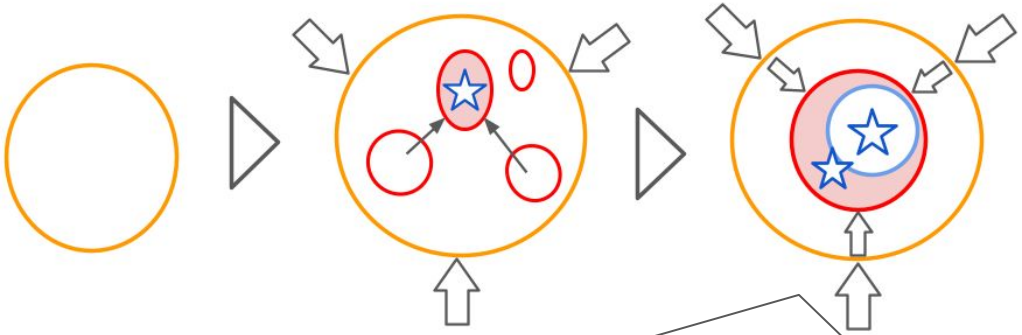

Hierarchical Structure: Interaction increases density → massive star formation
Confinement withstands feedback → Sustains clustered star formation

# 6. Summary

Work

- Analyzed major Galactic star-forming regions using FUGIN data
- Classified structures into hierarchical (Leaf) and Isolated using Dendrogram

Results

- Hierarchical structures are denser and gravitationally bound. → **Favorable environment for star formation**
- Global structures contain multiple velocity components. → **Gravitational confinement induces internal collisions.**
- Strong correlation with IR intensity (8, 24 μm) and HII regions
  - Isolated: **Formation halts due to feedback (Gas dispersal).**
  - Hierarchical: **Formation is sustained by confinement from external layers.**

Conclusion

**Large-scale confinement and internal interactions sustain clustered star formation against feedback.**

**Observational support for the GHC-driven CCC scenario**

Future Work

Investigation of the nearby galaxy M33 to refine the evolutionary model

Comparison with high-resolution GPU hydro-simulations using the same analysis method

# Appendix

## List of Target Areas

| Area | Galactic Longitude [degree] | Galactic Latitude [degree] | Radial Velocity [km $s^{-1}$] | Distance [kpc] |
|---|---|---|---|---|
| G18.15-0.30+51 | 17.8 - 18.8 | -0.8 - 0.0 | 25 - 75 | 6.07 |
| G45.3+0.1 | 45.0 - 45.6 | -0.3 - 0.3 | 50 - 75 | 8.00 |
| M16 (eagle nebula) | 16.6 - 17.4 | 0.1 - 0.9 | 14 - 30 | 1.74 |
| M17 | 14.8 - 15.5 | -0.8 - -0.3 | 0 - 30 | 1.98 |
| N4 | 11.8 - 12.0 | 0.7 - 1.0 | 20 - 30 | 2.80 |
| N14 | 13.7 - 14.9 | -0.6 - 0.1 | 30 - 50 | 3.10 |
| N35 | 24.1 - 24.7 | -0.1 - 0.5 | 100 - 130 | 8.80 |
| W33 | 12.5 - 13.5 | -0.5 - 0.5 | 15 - 60 | 2.40 |
| W42 | 25.5 - 26.0 | -0.5 - 0.0 | 85 - 125 | 3.80 |
| W43 | 30.2 - 31.2 | -0.5 - 0.5 | 70 - 120 | 5.49 |
| W49N | 42.8 - 43.4 | -0.4 - 0.2 | -5 - 20 | 11.11 |
| W51A | 48.7 - 49.7 | -0.7 - 0.3 | 40 - 75 | 5.40 |

# Appendix

## Resolution Correction

| Area | Distance [kpc] | Resolution [arcsec] |
|---|---|---|
| G18.15-0.30+51 | 6.07 | 37 |
| G45.3+0.1 | 8.00 | 28 |
| M16 (eagle nebula) | 1.74 | 128 |
| M17 | 1.98 | 112 |
| N4 | 2.80 | 79 |
| N14 | 3.10 | 72 |
| N35 | 8.80 | 25 |
| W33 | 2.40 | 93 |
| W42 | 3.80 | 58 |
| W43 | 5.49 | 40 |
| W49N | 11.11 | 20 |
| W51A | 5.40 | 41 |

Using imsmooth by CASA, the resolution is corrected according to distance and the spatial scale is unified.

Aligned with the farthest target, W49N (11.11 kpc), the corrected resolution of a target at a distance $d$ of 1000 kpc is $20'' \times (11.11/d)$

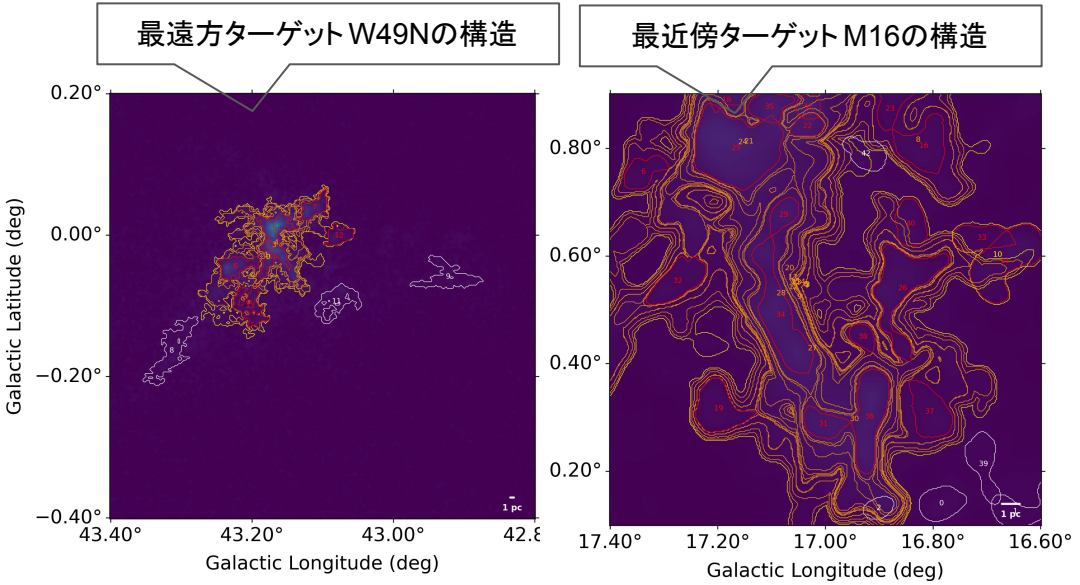

# Appendix

## Column Density Calculation (Excitation Temperature)

$$\begin{aligned}\Delta I_{12} &= (1 - e^{-\tau_{12}})(B_\nu(T_{\rm ex}) - B_\nu(T_{\rm bg})) \\ &= (B_\nu(T_{\rm ex}) - B_\nu(T_{\rm bg})) \qquad \because \tau_{12} \gg 1\end{aligned}$$

$$\Delta I_{12} = \frac{2k\nu_{12}^2}{c^2} T_{\rm peak} \quad B_\nu(T) = \frac{2h\nu_{12}^3}{c^2} \frac{1}{e^{h\nu_{12}/kT} - 1}$$

$$\begin{aligned}\therefore T_{\rm peak} &= \frac{h\nu_{12}}{k} \frac{1}{e^{h\nu_{12}/kT_{\rm ex}} - 1} - \frac{h\nu_{12}}{k} \frac{1}{e^{h\nu_{12}/kT_{\rm bg}} - 1} \\ &= \frac{5.53}{e^{5.53/T_{\rm ex}} - 1} - 0.819\end{aligned}$$

$$\Rightarrow T_{\rm ex} = \frac{5.53}{\ln\left(1 + \dfrac{5.53}{T_{\rm peak} + 0.819}\right)}$$

# Appendix

## Column Density Calculation (Optical Thickness)

$$\Delta I_{13} = (1 - e^{-\tau_{13}})(B_\nu(T_{\rm ex}) - B_\nu(T_{\rm bg}))$$

$$\Rightarrow \tau_{13} = -\ln\left(1 - \frac{\Delta I_{13}}{B_\nu(T_{\rm ex}) - B_\nu(T_{\rm bg})}\right)$$

$$\Delta I_{13} = \frac{2k\nu_{13}}{c^2} T_{\rm b}$$

$$\tau_{13} = -\ln\left(1 - \frac{T_{\rm b}}{\frac{h\nu_{13}}{k}\frac{1}{e^{h\nu_{13}/kT_{\rm ex}} - 1} - \frac{h\nu_{13}}{k}\frac{1}{e^{h\nu_{13}/kT_{\rm bg}} - 1}}\right)$$

$$= -\ln\left(1 - \frac{T_{\rm b}}{5.29(J - 0.164)}\right), \quad J = \frac{1}{e^{5.29/T_{\rm ex}} - 1}$$

# Appendix

## Column Density Calculation (Column Density)

$$N_{13} = \frac{3k}{8\pi^3 \mu^2 B} \frac{T_{\rm ex} + 0.88}{1 - e^{-h\nu_{13}/kT_{\rm ex}}} \int \tau_{13} dv$$

$$= 2.42 \times 10^{14} \frac{T_{\rm ex} + 0.88}{1 - e^{-5.29/T_{\rm ex}}} \int \tau_{13} dv$$

Here, partition function is $Q = \sum_J (2J+1) e^{-\frac{E_J}{kT_{\rm ex}}} \sim \frac{kT_{\rm ex}}{hB} + \frac{1}{3} \sim T_{\rm ex} + 0.88$

$$N_{\rm H_2} = 5.0 \times 10^5 N_{13}$$ （Dickman 1978）

# Appendix

## Result of G18.15-0.30+51

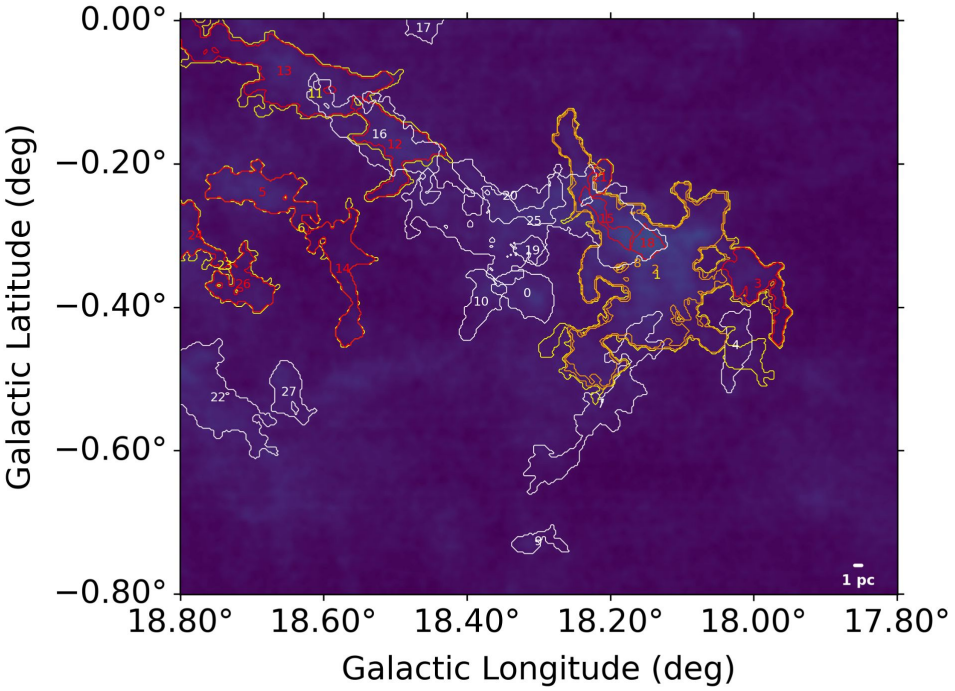


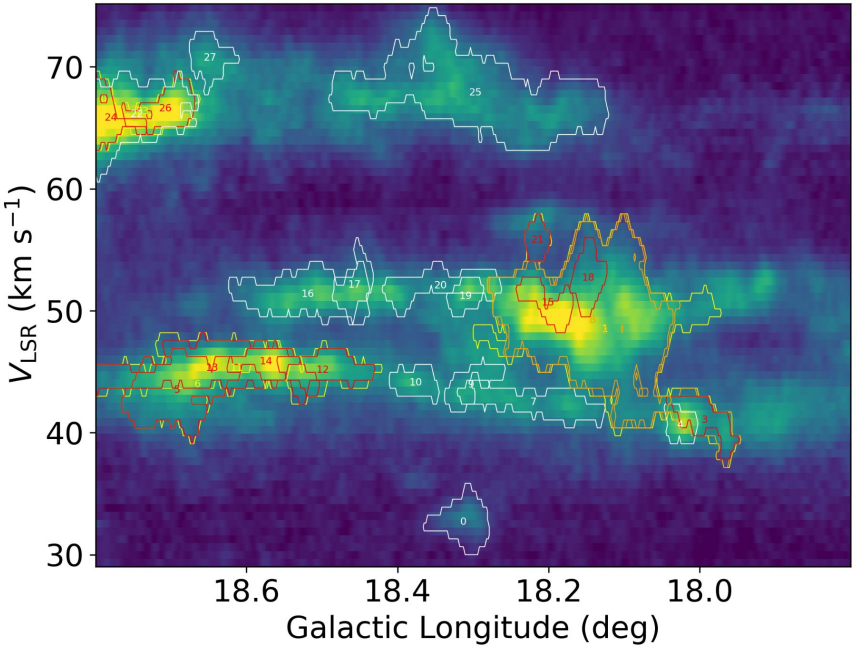

# Appendix

## Result of G45.3+0.1

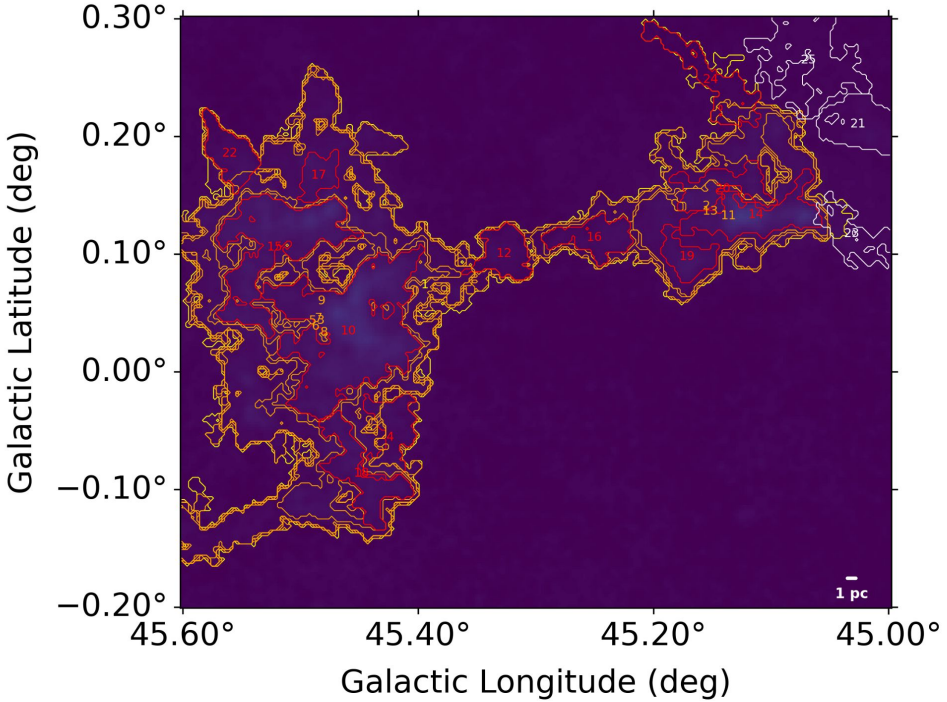


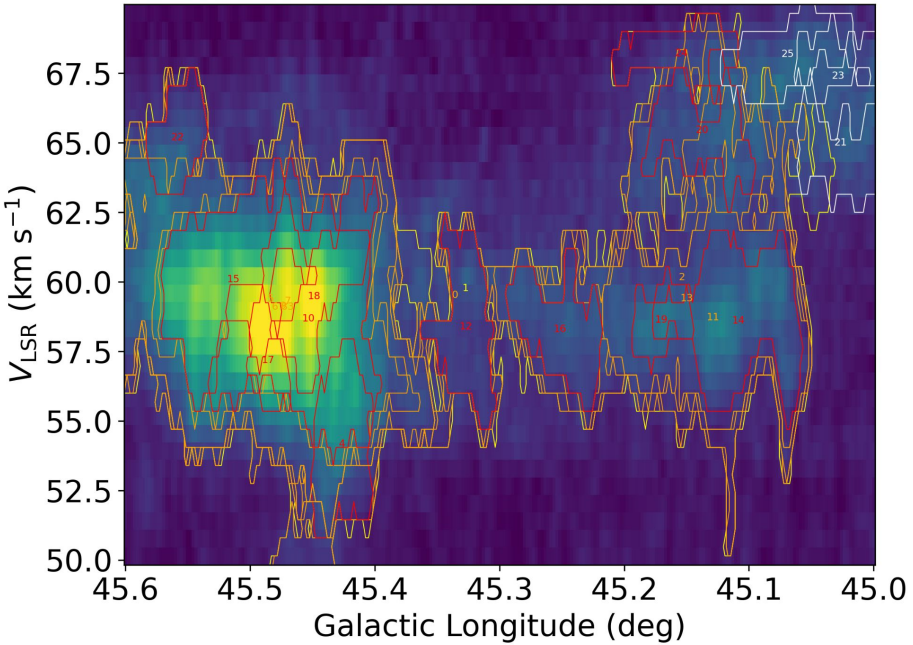

# Appendix

## Result of M16

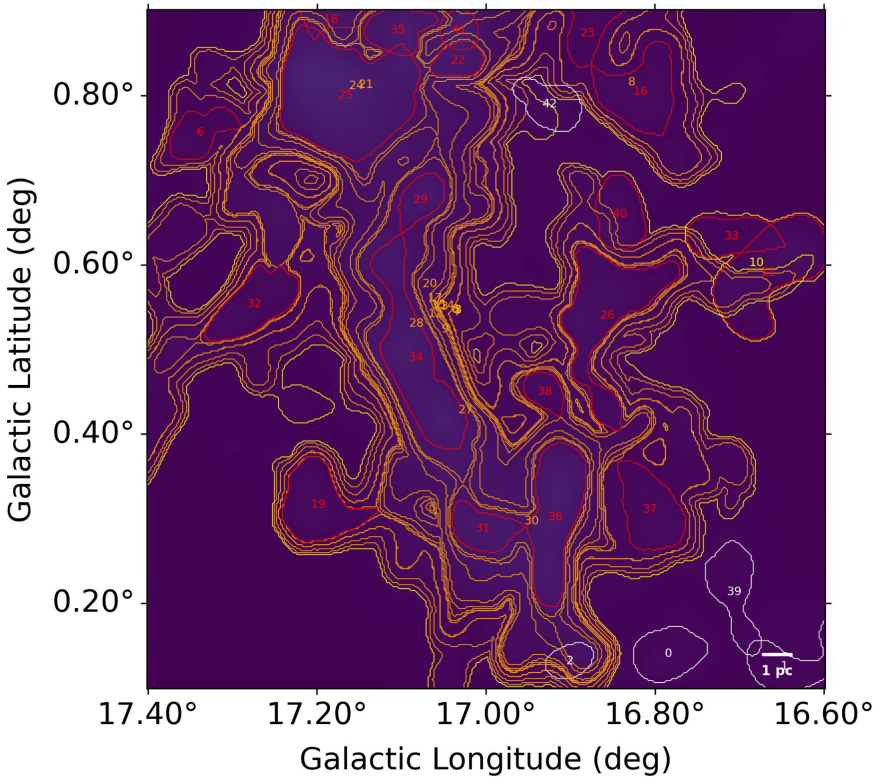


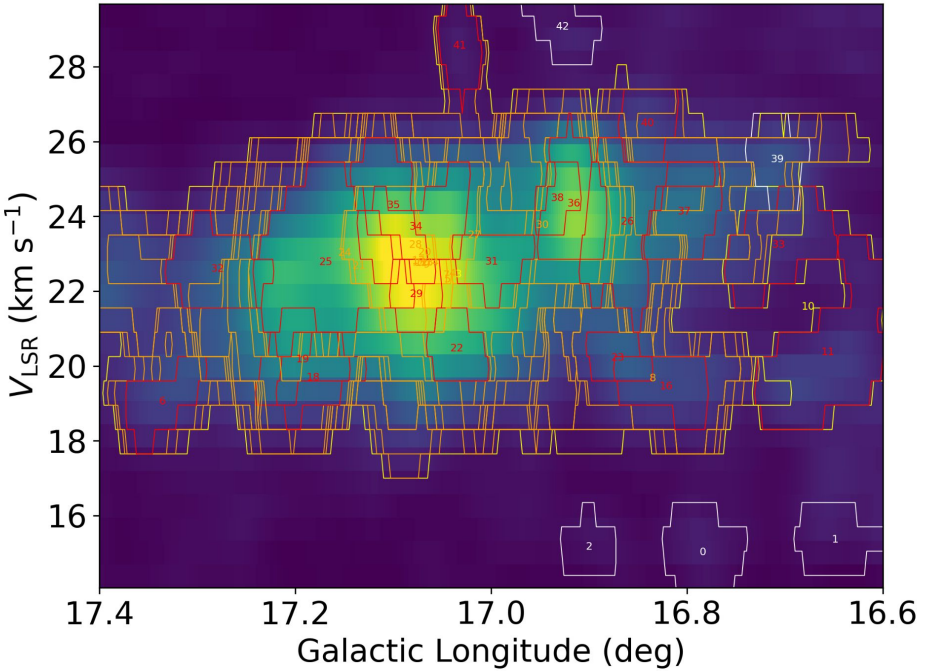

# Appendix

## Result of M17

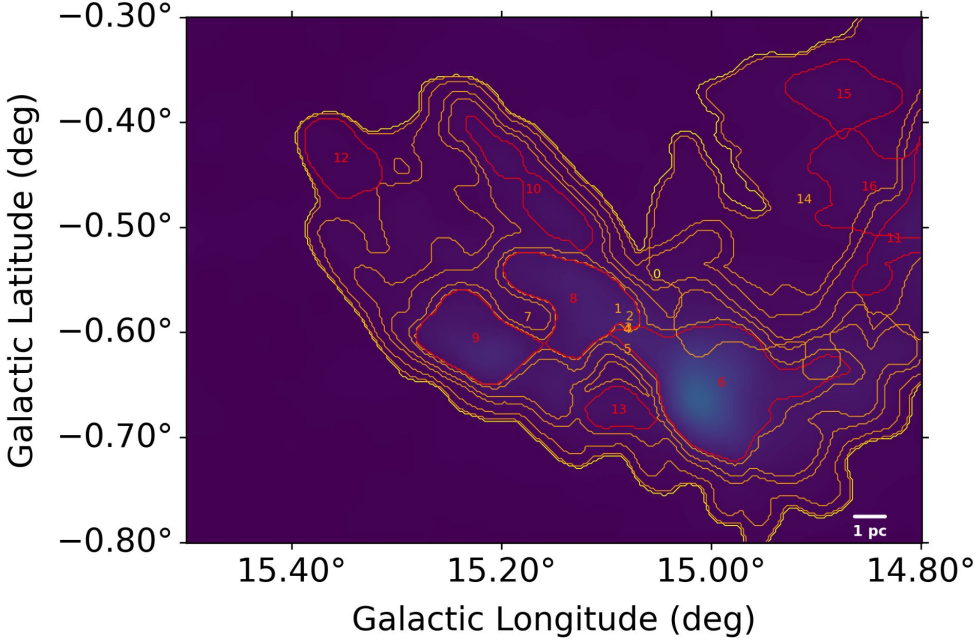


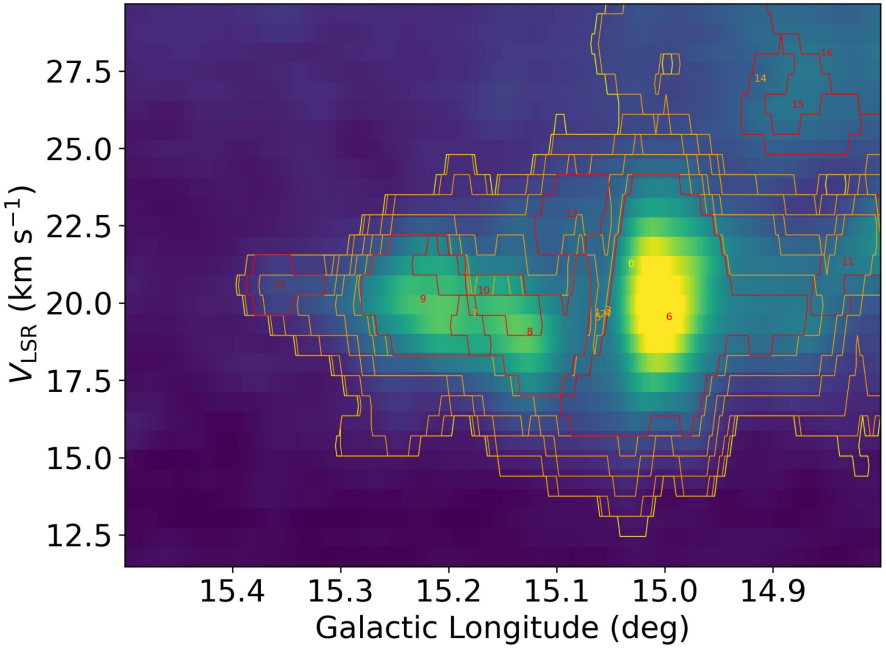

# Appendix

## Result of N4

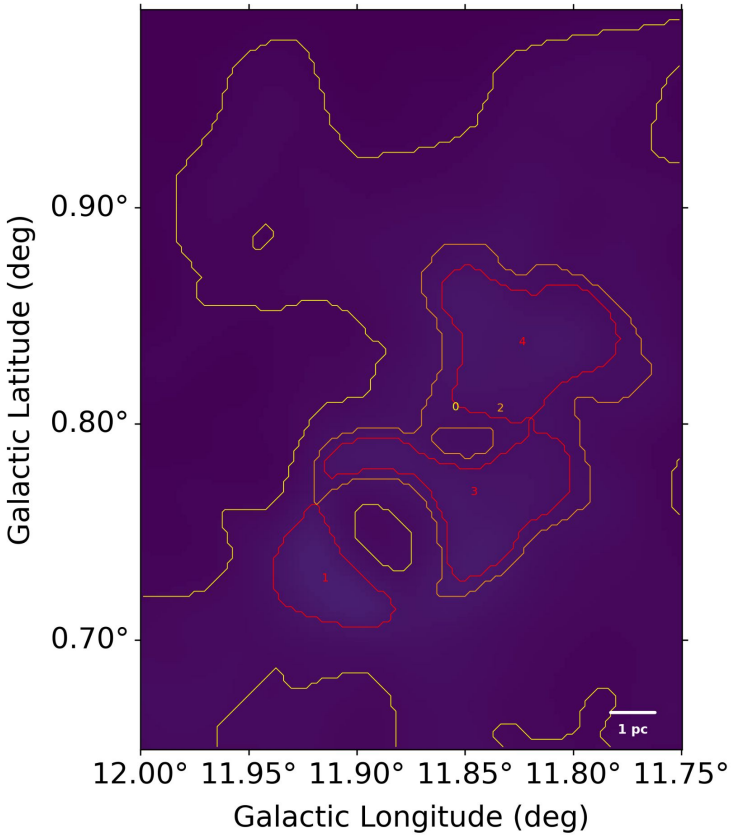


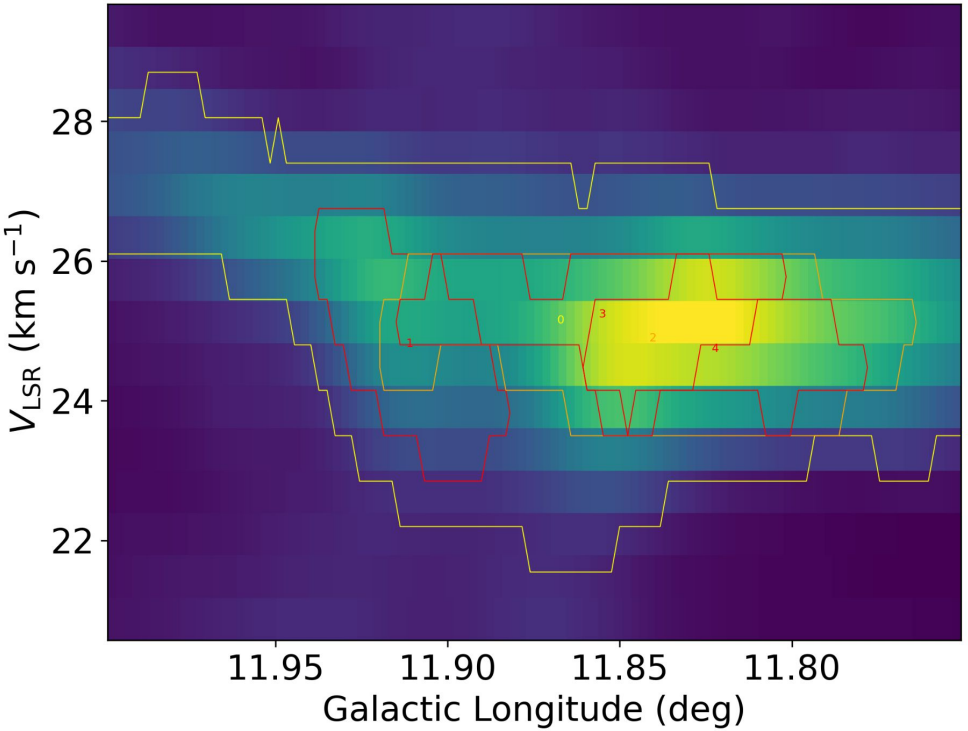

# Appendix

## Result of N14

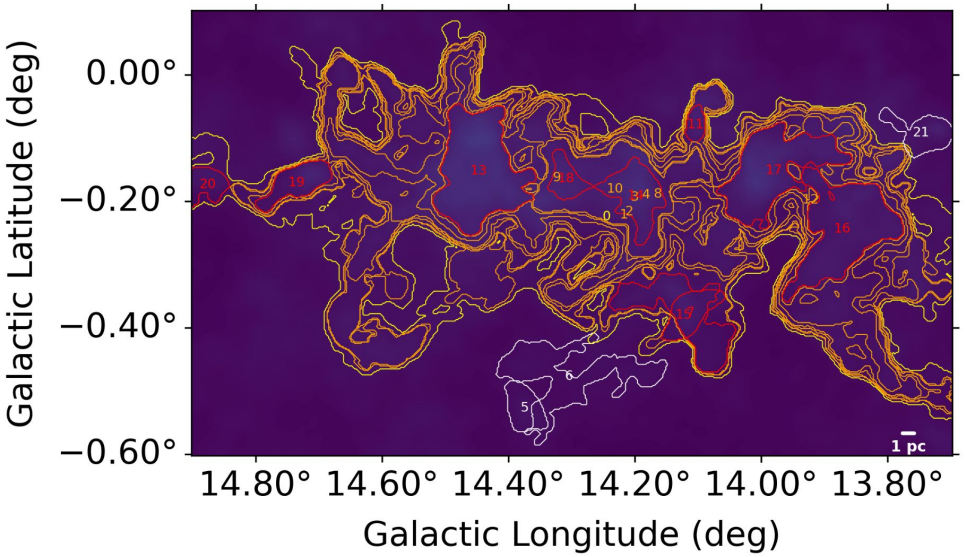


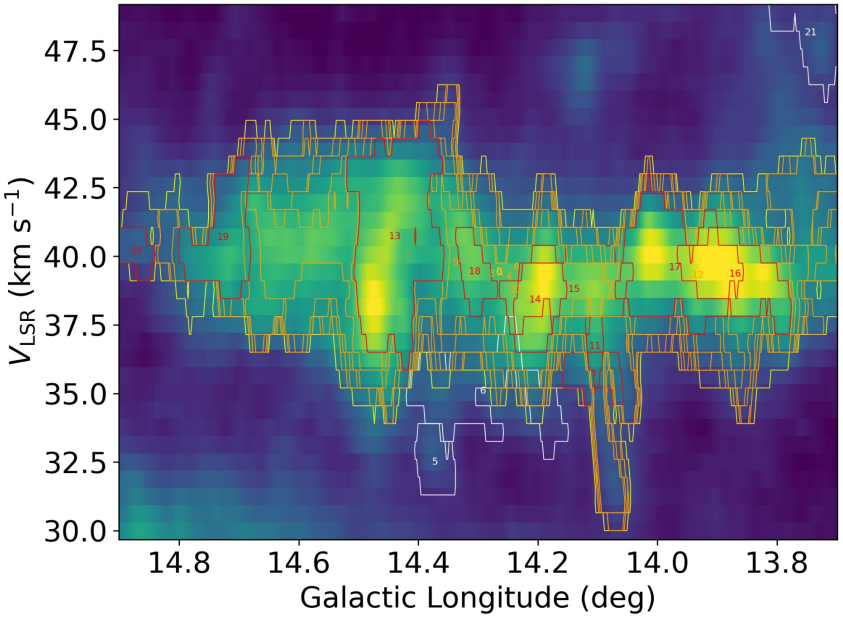

# Appendix

## Result of N35

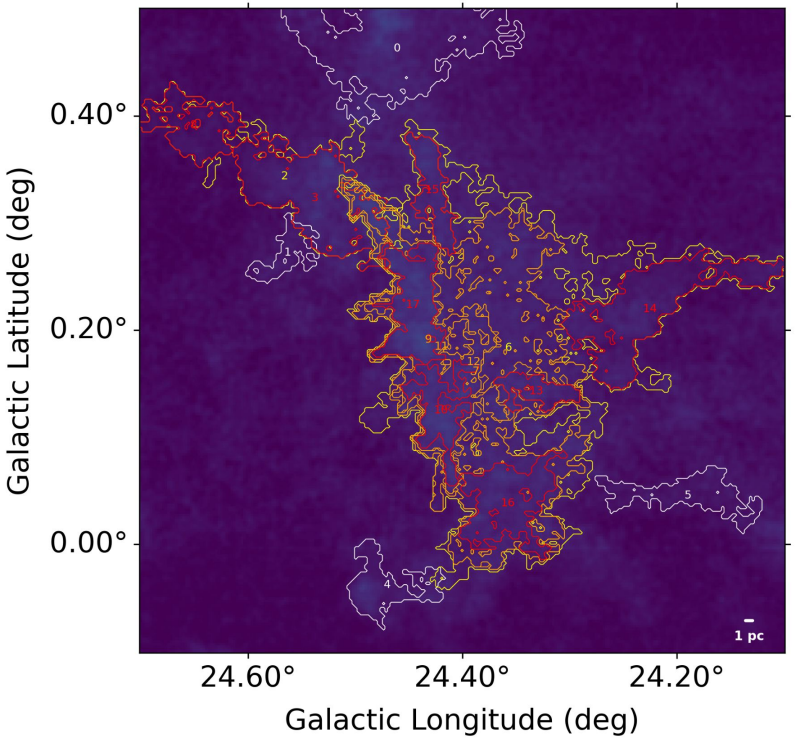


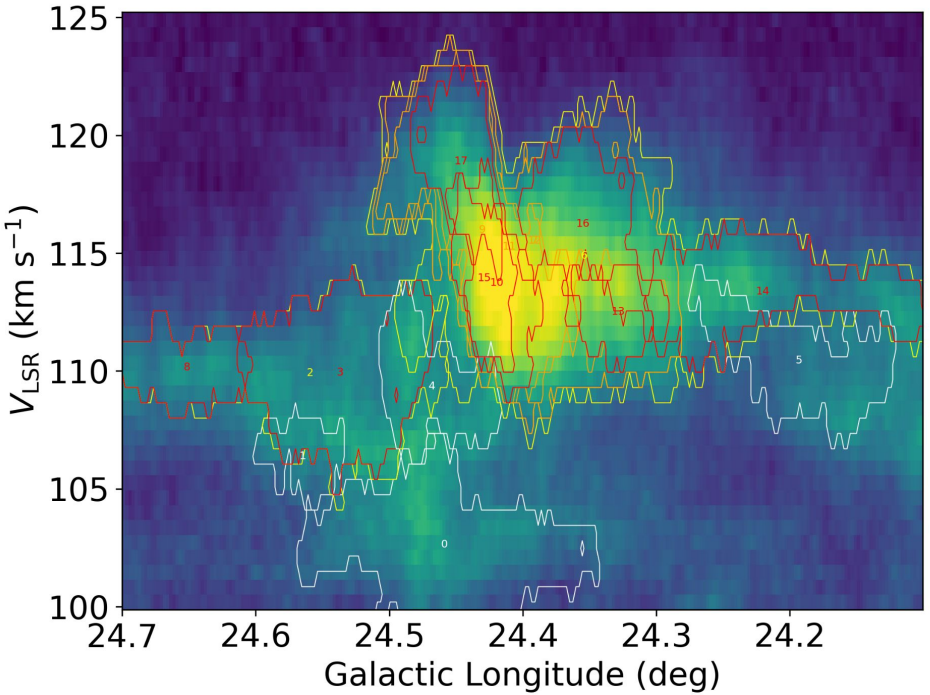

# Appendix

## Result of W33

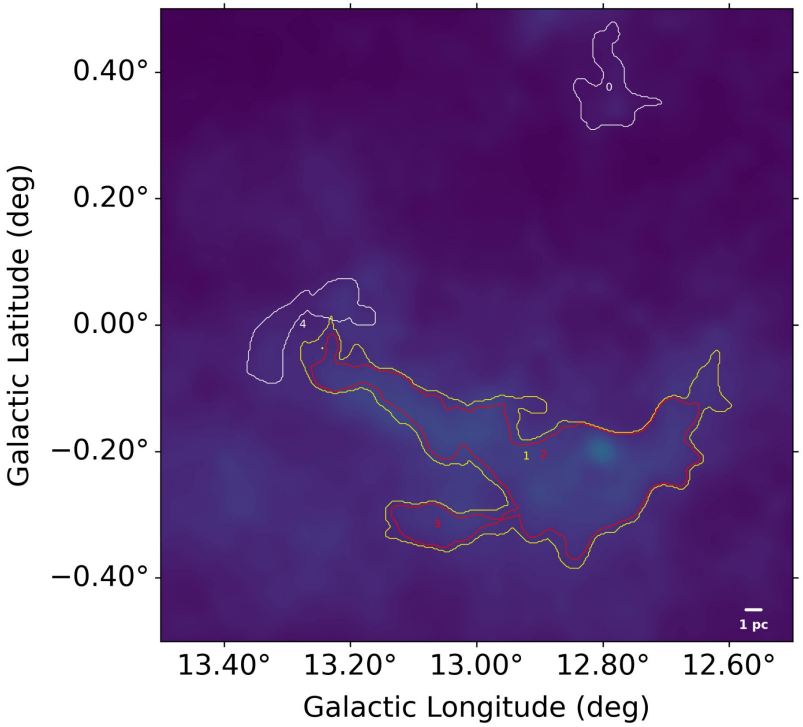


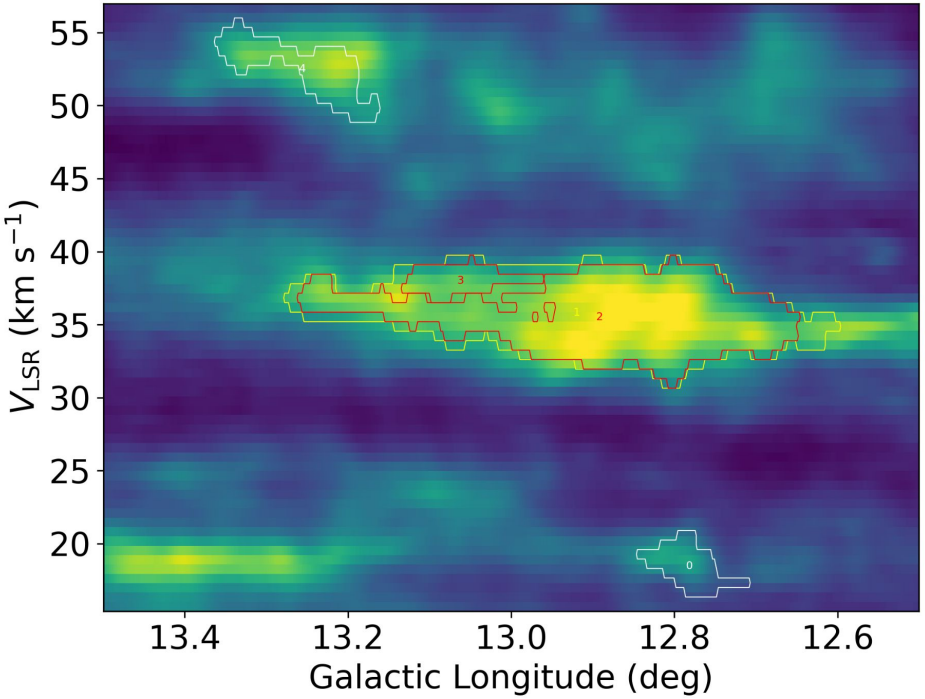

# Appendix

## Result of W42

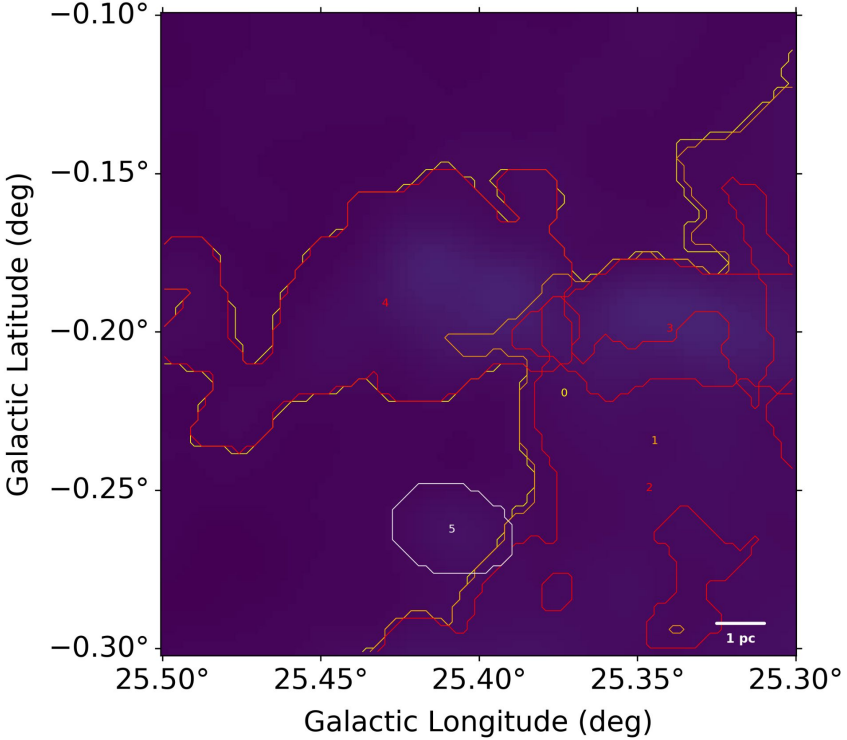


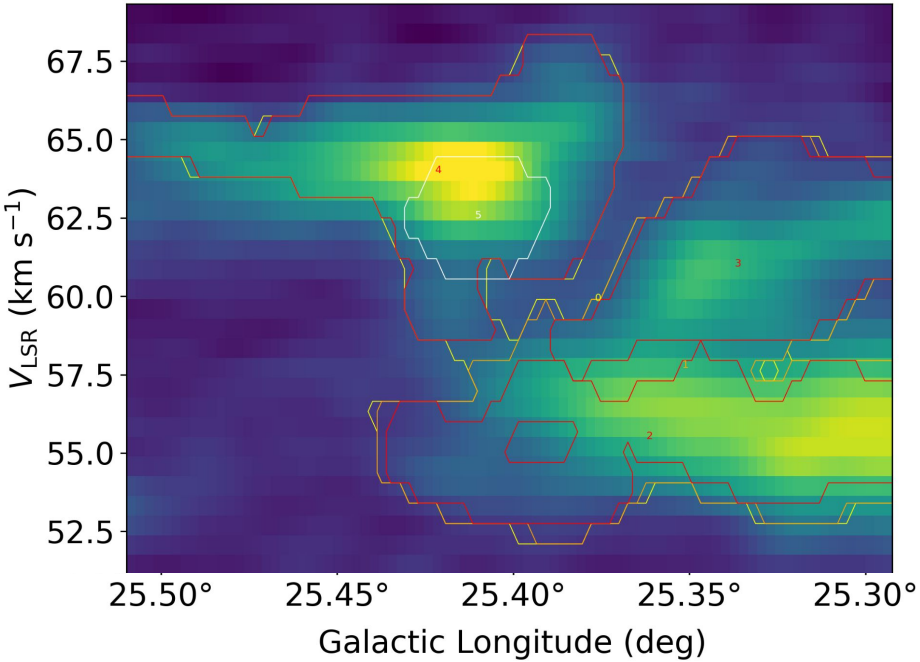

# Appendix

## Result of W43

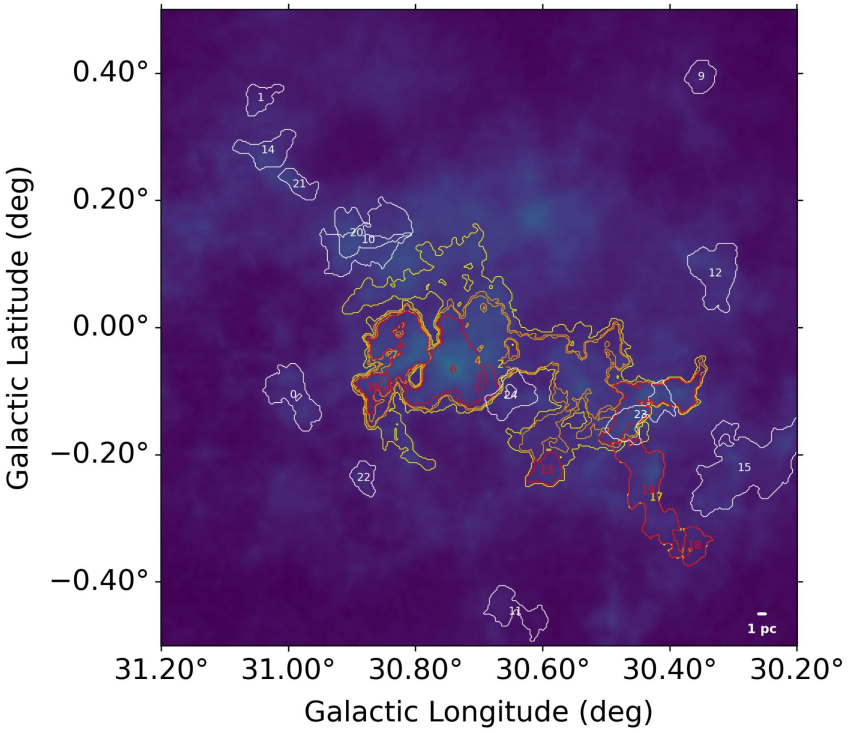


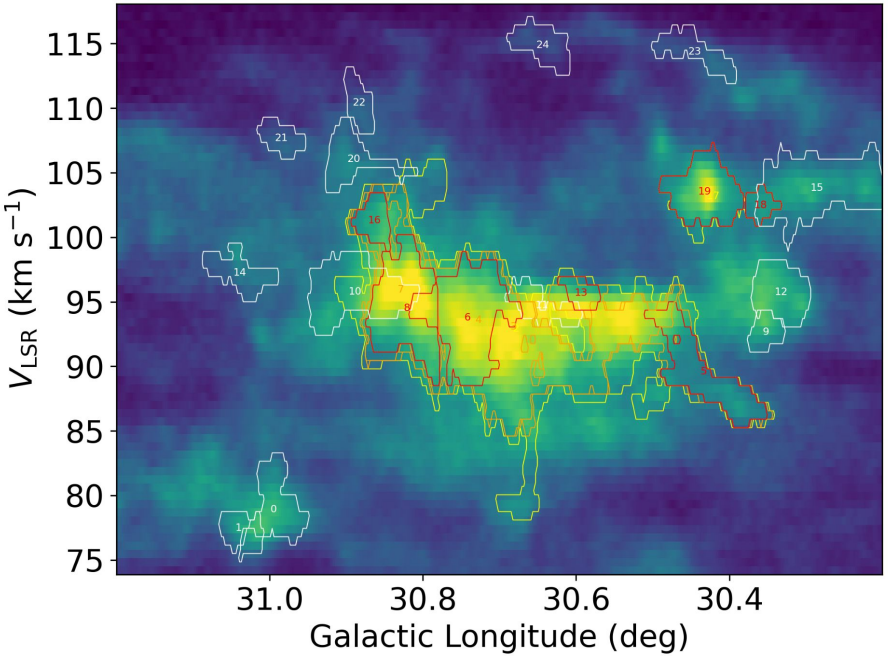

# Appendix

## Result of W49N